Experiments in Fluids (2023) 64:103
https://doi.org/10.1007/s00348-023-03628-5

RESEARCH ARTICLE

Experimental analysis of droplet coalescence and transport mechanisms on a single vertical fiber

Alexander Schwarzwälder[1] · Jörg Meyer[1] · Achim Dittler[1]

Received: 1 July 2022 / Revised: 28 March 2023 / Accepted: 29 March 2023

Abstract
In mist filtration, fiber-based coalescers are an established form of filtering droplets contained in mist. The filtration process can be divided into different process steps, describing the impact of the droplets on fibers, the formation of fluid structures and the liquid transport. In order to investigate mechanisms inside depth filters on a microscopic level, investigations are often reduced to single fibers. In this work, the coalescence and transport mechanisms of axially distributed water droplets on a vertical fiber, subjected to gravity, are reported. This is done with the latest high-speed camera technology commercially available. Automated tracking of droplets is used for a frame-by-frame investigation of droplet position, size, and oscillation. Coalescence mechanisms describe the process of fluid formation. The first observed coalescence mechanism is identified by the coalescence of droplets contained in mist with an adhering droplet at the fiber. The second coalescence mechanism describes the coalescence of two closely spaced sessile droplets on a fiber. As a result, the newly formed droplet oscillates and can begin to drain. Furthermore, the coalescence process of a draining and sessile droplet is reported. Both the draining droplet and the second droplet involved in the coalescence event can be subject to oscillation. The given temporal high-resolution information about the droplet position and deformation improves the understanding of droplet coalescence on fibers and by that also its influence on transport processes and therefore droplet drainage. Observed transport mechanisms which take part in the drainage process are gravitational draining, droplet bouncing, and droplet sweeping.

1 Introduction

Fiber-based coalescers are often used to remove droplets contained in mist for various applications ranging from water purification and food processing to oil refinery and gas-plants processes. Droplets are deposited on the fibers in the filter medium and collected there. On contact with adjacent droplets, these coalesce into larger droplets. Droplet-shaped liquid structures (clamshell and barrel shaped droplets) are formed as well as so-called liquid sails. Liquid sails can be spanned between adjacent fibers, when enough liquid is accumulated, which cover often a larger area inside the filter (Straube et al. 2021). The resulting structures and the deposition behavior depend on the media properties of the fiber (pore size, fiber diameter, fiber orientation, wetting behavior), the fluid properties (viscosity, density, surface tension) and operating parameters (temperature, pressure, gas velocity).

When the conditions are right, droplets can be transported along or removed from a fiber by different transport mechanisms illustrated in Fig. 1. Known transport mechanisms leading to droplet movement along the fiber are gravitational draining, and mobilization caused by pressure and shearing forces (Ojaghlou et al. 2018; Dawar and Chase 2008, 2010; Gilet et al. 2010). Another liquid redistribution and therefore transport mechanism is known from the droplet coalescence of unequal sized droplets on flat surfaces (Chu et al. 2016). A smaller droplet can hereby be swept toward the larger droplet. Chu et al. (2016) name this behavior droplet sweeping which might also occur with droplets on a fiber but has not been reported for such a case until now (Ojaghlou et al. 2018; Dawar and Chase 2010; Gilet et al. 2010; Mullins et al. 2007; Mead-Hunter et al. 2012). According to investigations of droplet collisions in gaseous environments, the droplets do not have to merge, but can also bounce off each other (Abouelsoud and Bai 2021; Tang et al. 2012; Pan et al. 2008; Qian and Law 1997). Qian and Law (1997) assume that a gaseous phase

✉ Alexander Schwarzwälder
alexander.schwarzwaelder@kit.edu

[1] Institute of Mechanical Process Engineering and Mechanics (MVM), Karlsruher Institute of Technology (KIT), Straße Am Forum 8, Karlsruhe, Germany

Published online: 12 May 2023

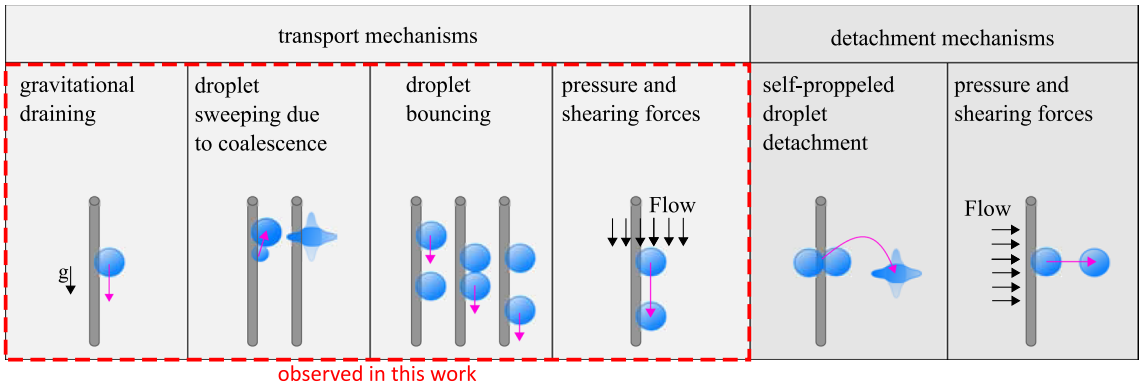

Fig. 1 Transport and detachment mechanisms of droplets on a vertical fiber. Purple arrows indicate the movement of the droplet

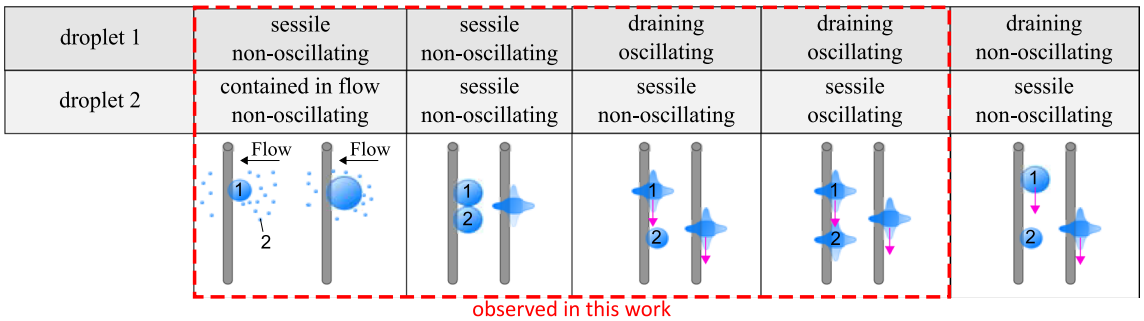

Fig. 2 Coalescence mechanisms of droplets on a vertical fiber

can be trapped between two colliding droplets. When the inertia is high enough the gas between droplets is squeezed out. Below a distance of 10^2 Å molecular interaction initiates the coalescence. When the inertia is not high enough, kinetic energy is converted into surface tension energy. By attempting to restore the spherical shape, the droplet bounces away. It is worth noting that bouncing of water droplets in an environment of 1 atm pressure was not observed so far.

Depending on the boundary conditions, the droplet movement does not have to be along the fiber. Droplets can also be removed from the fiber by shearing forces (Dawar and Chase 2010), or self-propelled droplet removal by coalescence (Zhang et al. 2015). Zhang et al. (2015) observed self-propelled droplet detachment from the fiber in the case of a vertical fiber orientation when droplets are arranged in the circumferential direction at the same axial position. This mechanism was studied in high temporal resolution. Pronounced droplet deformation was observed. Furthermore, it was investigated that water droplets of the same size do not detach from a hydrophobic plane when coalescing. Therefore, it is important to study the coalescence process on filter structures such as fibers if one wants to study the drainage and detachment process; a simplified examination of droplet coalescence on flat surfaces or in void space is not sufficient.

Naturally, in coalescence filters not only the process of fluid transport but also the coalescence process is of great importance. Several coalescence mechanisms can be identified on a vertical single fiber that is continuously exposed to a stream of mist and are illustrated in Fig. 2.

First, droplets contained in mist are deposited on fibers and later on coalesce also with already deposited larger droplets and lead to a continuous growth of the larger droplets. This mechanism has been observed by many other investigations. Many of the investigations focused on the filter performance or the resulting liquid structure (Straube et al. 2021; Kampa et al. 2014; Hurwitz 2012; Mead-Hunter et al. 2013). Mead-Hunter et al. (2013) simulated for a portion of a coalescing filter the processes steps of droplet capture, coalescence, film break-up, and the motion of coalesced liquid droplets in coalescing filters. However, no detailed information about the coalescence mechanisms of droplets is given with a high temporal resolution by mead-Hunter et al., although the simulation should provide such information.

Secondly, the coalescence of a draining droplet with another sessile droplet on a vertical fiber was observed before but not investigated with high temporal resolution (Labbé and Duprat 2019). Several scenarios for the coalescence mechanism of a draining and sessile droplet on a fiber are possible. First a droplet draining along the fiber might

not oscillate until its first time coalescing with another droplet. The movement of a single non-oscillating droplet downward a vertical fiber was investigated by Gilet et al. (2010). As known from droplet coalescence on fibers (Zhang et al. 2015), flat surfaces (Zhang et al. 2015; Jin et al. 2017), and gaseous environments (Lycett-Brown et al. 2014), a droplet starts to oscillate due to coalescence and therefore a draining droplet can also oscillate when interacting with sessile non-oscillating droplets. The last less likely scenario would be the coalescence of two oscillating droplets but was still observed in this work. Additionally, it should be mentioned at this point that depending on the Reynolds number sessile clamshell droplets can also oscillate in radial and transversal direction on fibers (Mullins et al. 2005). For droplet radii between 100 µm and 450 µm, the activation of oscillation occurs at Reynolds numbers between 50 and 100. For this kind of oscillation, no transient deformation of the droplet was observed.

When fibers are used for the separation of mist, a droplet chain of closely spaced droplets is created. At a certain size, these sessile droplets will be large enough to come into contact and coalesce. Deka et al. (Deka et al. 2019) observed for unequal sized water droplets in air with neglectable collision speed, so for coalescence of two resting droplets, that the expansion of the coalesced droplet is wider than that of the two initial droplets. If this is also valid for the coalescence of sessile droplets on a fiber than this could cause a chain reaction of coalescence events of closely spaced droplets on a fiber. Zhang et al. (Zhang et al. 2022) used two needles to position two droplets side by side on a horizontal fiber. According to their results, the influence of the fiber on the formation of the bridge can be neglected. The used needles prevented in their case the coalesced droplet from deforming dynamically in the direction along the axis of rotation of the liquid bridge.

Further investigations of the coalescence process were conducted independently of filtration issues with droplets fixed to needles. This research mostly focuses on the initial process during coalescence, where a liquid bridge is formed between two droplets (Zhang et al. 2022; Chen et al. 2015; Chireux et al. 2015, 2021; Thoroddsen et al. 2005; Paulsen 2013). The bridging process is determined by the differing Laplace pressure and surface tension when two droplets come into contact due to jump-to-contact instability based on van der Waals forces. This leads to a topology change at the contact area which is linked to a singularity of the dynamics (Paulsen et al. 2012). It has long been assumed that there are two resulting dynamical regimes, a viscous regime, which dominates when the radius of the liquid bridge is small enough, and an inertial regime, when viscous effects become negligible with increasing radius. A current discussion about the initial regimes in the microscopic area of bridge formation shows the complexity of the mechanisms involved and that questions about the true regime and the initial coalescence process are not fully understood as of now (Chireux et al. 2021; Paulsen 2013; Paulsen et al. 2012, 2011).

Additionally, many investigations were carried out on the collision of freely moving droplets (Deka et al. 2019; Finotello et al. 2017; Li and Fritsching 2011; Pan and Suga 2005; Mansouri et al. 2014). These works focused on droplet collision and the outcome after collision and therefore the time-dependent deformation of the coalesced droplet until a clear outcome of the collision could be identified. Here, three regimes for the outcome of the droplet collision can be named: bouncing, coalescence, and separation. Depending on the collision velocity, the properties of the droplets (density, surface tension, diameter, viscosity) and the properties of the surrounding media the outcome after collision can differ. With increasing Weber number, the outcome after collision changes from coalescence after minor deformation to bouncing to coalescence after substantial deformation followed by separation (Li and Fritsching 2011).

No investigations with high temporal resolution could be found for the case of axially distributed droplets on a vertical fiber. In this work, the fundamental coalescence and transport mechanisms of axially adjacent positioned droplets on a vertical fiber are shown for the first time with high temporal resolution.

2 Materials and experimental setup

A metallic fiber (60.8% iron, 15.2% chrome, 10.5% carbon, 10.1% nickel, 3.3% others) with a diameter of 40 µm is used for the experiments. The droplet has a volume of 1.25 nl. The droplet contour above the triple point was approximated with a polynomial of third order. For this purpose, 100 pixels were used as sampling points above the triple point. The transverse static contact angle between the fiber and the tangent of the polynomial fit at the triple point is $85.1 \pm 0.7°$ and is drawn in Fig. 3.

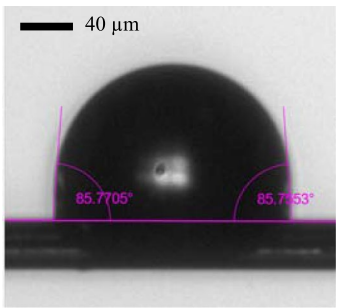

Fig. 3 Contact angle of water droplet on metallic fiber with a diameter of 40 µm

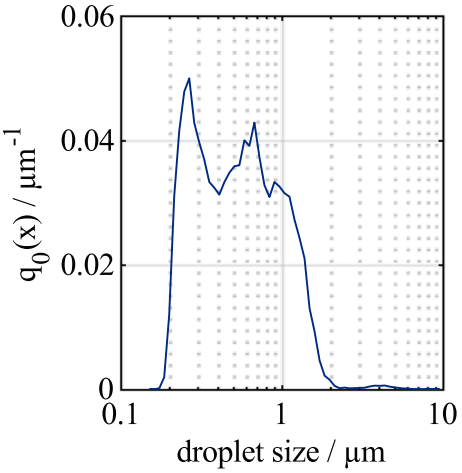

Fig. 4 Number-based density distribution of the droplets contained in the mist

To generate mist, particle-free, dry, compressed air is first moistened and then passed through a collision atomizer for atomization. Demineralized water is used for humidification and atomization. The compressed air has an overpressure of 1100 hPa compared to the environment. The mist is emitted through a round opening with a diameter of 8 mm and directed as a free jet onto the fiber. The number-based density distribution of the droplets contained in the mist is measured with a PALAS Promo 2000 with a welas 2100 H in a separate repeat experiment under same conditions. The distribution is shown in Fig. 4.

The vertically clamped fiber is located at a distance of 20 mm from the opening. In a repeat test, the measuring device (Testo 400) for determining the relative humidity, inflow velocity, temperature, and absolute pressure is mounted at the same position where the fiber was located. The corresponding experimental setup can be seen in Fig. 5. The operating parameters were kept constant during the experiment (relative humidity: 60±0.89%, velocity: 1.76±0.02 ms^{-1} temperature: 16.45±0.40 °C, absolute pressure: 986.44±0.05 hPa). The direction of observation is perpendicular to the incident flow. A high-speed camera in combination with a diffuse backlight is used for recording the processes at 10,000 fps. The magnification of the lens is 1.65. During the entire observation time, the incident flow with mist was switched on.

3 Methods

To investigate the development of the droplet distribution over time, a high-speed camera was used and droplets were tracked and evaluated regarding size and position. To track the droplets, the individual frames of the recorded video must be pre-processed before handing over to the tracker. The individual steps of the workflow are shown in Fig. 6. The first image on the left side in Fig. 6 shows the original raw greyscale image taken with the camera. In the first

Fig. 5 Experimental setup

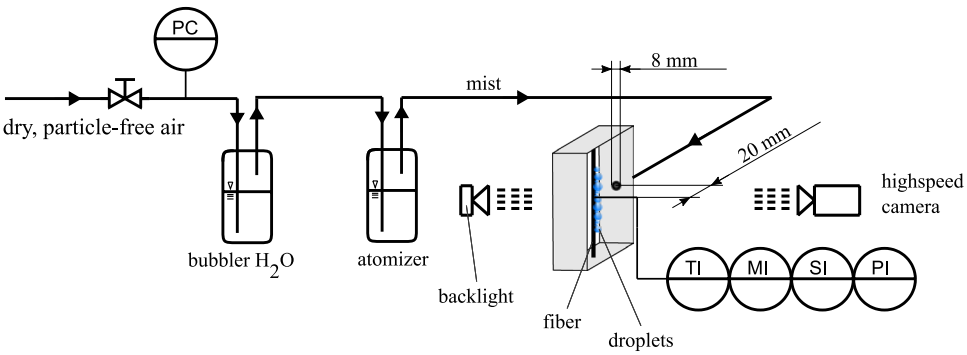

Fig. 6 Steps of the frame by frame image pre-processing procedure for tracking multiple droplets on a fiber

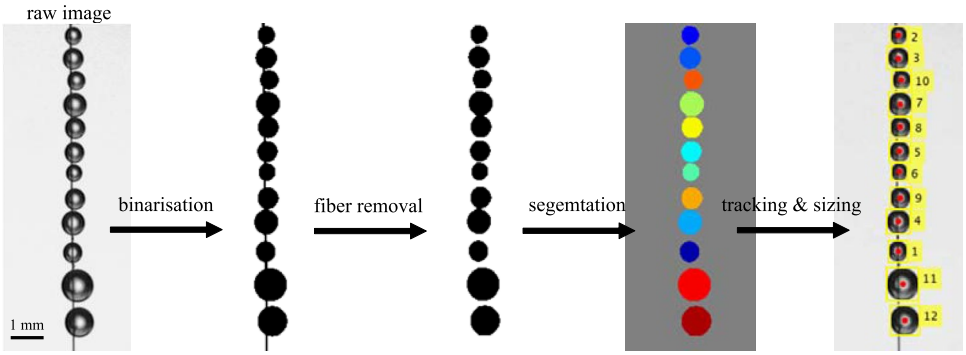

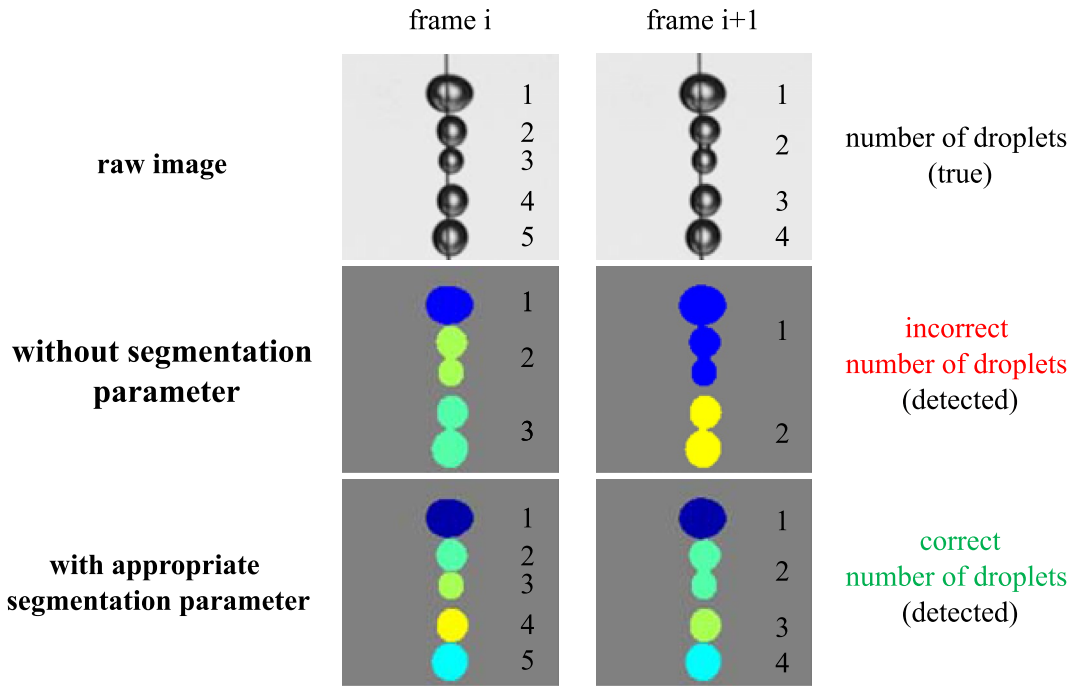

Fig. 7 Illustration of the influence of the separation parameter used in the image processing for automated tracking. Each different color in an image represents a detected droplet

processing step, the greyscale image is converted into a binary image based on a threshold value so that the background appears white and the foreground black. This creates a sharp interface between the droplet's contour and the background. By that the droplet dimensions can be determined later on. In the second image processing step the fiber is removed by a customized filter: If the number of black pixels in a horizontal pixel row is less than or equal to the number of pixels of the fiber diameter, these black pixels are inverted. Furthermore, the droplets must be segmented so that the tracking tool can treat each single droplet as a single object. This is done by splitting the pixel region of all droplets with the *watershed* function in Matlab. Additionally, in this processing step a sensitivity parameter is introduced which controls the segmentation of closely spaced droplets. The sensitivity parameter was created in Matlab using the function *bwdist* and *imhin*. The need of the sensitivity parameter is illustrated in Fig. 7. The segmented pixel regions, respectively, the droplets are then evaluated with respect to the center of mass and maximal dimensions in x- and z-direction ($x_{\max}$ and $z_{\max}$). These values are passed to the tracking tool.

The automated tracking tool is based on a constant-velocity Kalman filter and was implemented with the tracking toolbox in MATLAB. Each newly detected droplet is assigned to a track with a corresponding TrackID immediately in the frame in which it is identified without any lead time and kept as long as this droplet is detected in the following frame. The TrackID is highlighted in yellow in Fig. 6. As soon as a registered droplet is not detected in a subsequent frame, this TrackID is immediately deleted. Due to the very reliable detection of the droplets, this type of track management is sufficient. Furthermore, the values for $x_{\max}$ and $z_{\max}$ are shown in form of a yellow enclosing box for the respective droplet against the background of the raw image in the right image of Fig. 6. The center of mass for each detected droplet is marked as a red dot.

The coordinate system and the orientation of the coordinate axis in relation to the fiber axis and the gravitational force is shown in Fig. 8. The z-axis points in the direction of the gravitational force. The x-axis points in the opposite direction to the inflow of mist. The maximal dimensions in x- and z-direction are used to calculated the average diameter D_i of the droplet using

$$D_i = \frac{\left(z_{\max,\,\mathrm{i}} + x_{\max,\mathrm{i}}\right)}{2}. \tag{1}$$

The index $i = s, l$ is used to notate the smaller (s) and larger (l) droplet. Dimensionless numbers such as the Weber (We) and Ohnesorge (Oh) number are typically used to characterize the collisions and coalescence of two droplets. The Weber number represents the ratio between inertial forces and surface tensions and is defined as

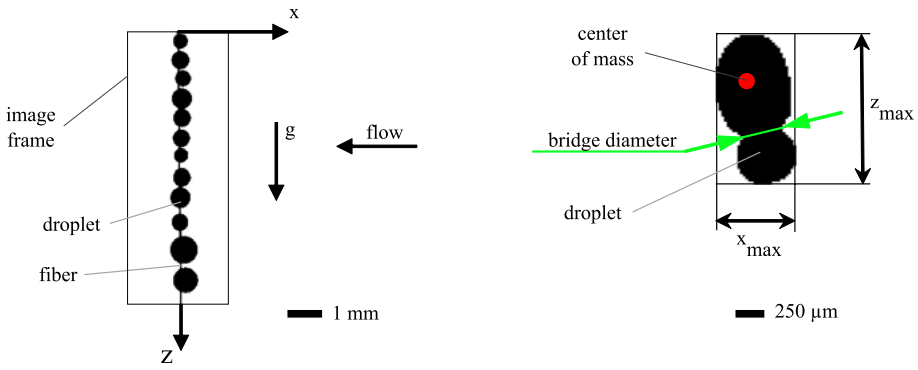

Fig. 8 Illustration of the used coordinate system (left) and the measured sizes x_{max}, z_{max}, the center of mass and bridge diameter of a coalescing droplet (right)

$$\mathrm{We} = \frac{D_s \rho_{liq} \left| u_{rel}^2 \right|}{\sigma}, \tag{2}$$

where D_s is the average diameter of the smaller droplet, ρ_{liq} the liquid density of the droplet, and σ the surface tension. u_{rel} describes the propagation speed of the droplet surfaces relative to each other before contact and can differ significantly from the usually used relative velocity of the center of mass for non-oscillating colliding droplets.

The Ohnesorge number describes the ratio of viscous forces to the square root of the product of inertial forces and surface tension. Different characteristic lengths are used when investigating droplet collision and the expansion of a liquid bridge at coalescence. For describing the collision of two droplets with Oh_C, the droplet diameter of the smaller droplet D_s is used, while describing bridging with Oh_B the minimum neck radius R_B is used. Therefore, one obtains

$$\mathrm{Oh}_C = \frac{\mu_{liq}}{\sqrt{\rho_{liq} \sigma D_s}} \tag{3}$$

$$\mathrm{Oh}_B = \frac{\mu_{liq}}{\sqrt{\rho_{liq} \sigma R_B}}. \tag{4}$$

The dynamic viscosity of the liquid droplet is notated as μ_{liq}.

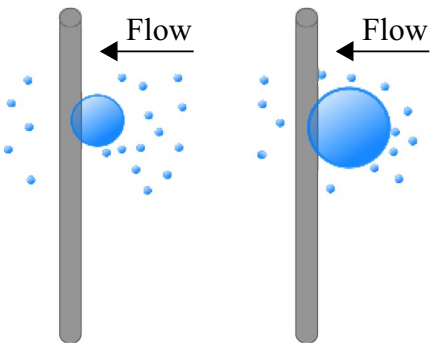

Fig. 9 Coalescence induced droplet growth

4 Results and discussion

In this work, observations were made with a high-speed camera for one camera position. Furthermore, one material combination was investigated with the mentioned metallic fiber and demineralized water as liquid. The droplet distribution formed by deposition of droplets from mist is a random variable that cannot be exactly reproduced repeatedly. Due to limited storage of the high-speed camera, not all process steps could be recorded in a single video. Therefore, the coalescence-induced droplet growth by mist deposition is recorded in one take. The droplet drainage is recorded in a separate repeated experiment under same conditions. A total of 5 high-speed video recordings of the deposition process up to the start of drainage and 9 recordings of the drainage process are evaluated. Standard deviations are given to the extent where it is possible. It should be remembered that the droplet distribution is a random variable and coalescence events happen therefore at different locations of the fiber at different times. Also, the droplet sizes, velocity, and state of deformation vary for each coalescence event.

Coalescence-induced droplet growth by mist deposition as illustrated in Fig. 9 is well known and has been investigated by Labbé and Duprat (2019) in terms of the collection rate of individual fibers. In this work, coalescence-induced droplet growth is evident as a droplet chain is formed by deposition of droplets contained in the mist on the fiber and on droplets already deposited. The number of droplets for the time interval from an unloaded fiber to the first draining of a droplet is shown in Fig. 10 for five repeat experiments. The regressive behavior of the function curves agrees with each other in a good approximation. The value at the end of each plot describes the number of drops that remain on the fiber after the droplet has drained and coalesced with the drops on its path downward the fiber. The number of droplets inside the observed frame at the beginning of the drainage is 19 ± 1.67 in the and marked by the horizontal bar.

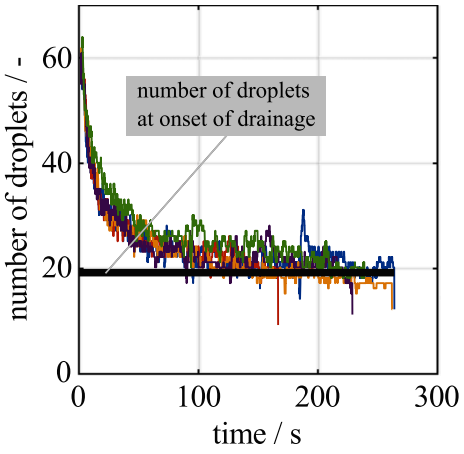

Fig. 10 Number of droplets on fiber (colored graphs) and number of droplets at beginning of drainage (horizontal line)

According to Fig. 11, a droplet chain has characteristic states during droplet growth. In the first state, the drops are almost the same size and lie close to each other. As the droplets continue to grow through coalescence with droplets of mist, closely neighboring droplets coalesce on the fiber to form larger droplets. Two neighboring droplets occupy more space in the axial direction of the fiber immediately before coalescence than a coalesced droplet formed from corresponding neighboring droplets. This results in a chain of drops in which there is a comparatively large distance between the drops. On the space between drops on the fiber that is freed up by the coalescence process, drops of the mist are immediately deposited again. Smaller drops can grow between larger drops.

Due to coalescence of the smaller drops with the larger drops, the larger drops continue to grow until they almost touch each other. No smaller droplets form between the larger droplets and a droplet chain of approximately homogeneous droplet size can be seen. The process of droplet growth and the associated reduction in the number of droplets on the fiber is repeated until the droplets are removed by detachment or transport mechanisms.

The larger the droplet size of an approximately homogeneous droplet distribution, the larger the empty spaces between the droplets after coalescence. Thus, the period duration of recurring characteristic droplet series also increases with increasing droplet size.

After all, this work is not about the study of coalescence-induced droplet growth. Instead, the focus of this work is on the coalescence and transport mechanisms for the onset of drainage and the drainage of a droplet itself along the fiber.

When two non-oscillating neighboring droplets on a fiber come into contact, they can coalesce and form an oscillating droplet as depicted in Fig. 2. The difference in size of the drops determines the movement of the centers of mass of both drops. If the drops are the same size, the centers of mass move evenly toward each other. If the droplets are not the same size are unequally distributed, the smaller droplet moves more than the larger drop. This is called droplet sweeping.

The coalescence of two droplets can be divided into two process steps: first, the formation and development of a liquid bridge between two droplets and second, the further development of the merged droplet in terms of deformation and oscillation.

The bridge development has been excessively investigated in the literature and is still a topic of current discussions (Chireux et al. 2021; Paulsen 2013; Paulsen et al. 2012, 2011). The literature agrees that at least two regimes exist, the stokes regimes, dominated by viscous effects and the inertial regime. The Ohnesorge number Oh_B is often used to determine the regime of the liquid (Chen et al. 2015; Chireux et al. 2021). At the initial contact, the dynamics are described by $Oh_B >> 1$, the Stokes regime. However, the Stokes regime was never observed experimentally for droplet of water coalescing in air. When R_B increases, Oh_B decreases and a transition to an inertial regime ($Oh_B << 1$) occurs. In this regime, the central part of the bridge can be observed as a cylindrical body (Chireux et al. 2021). The length of the liquid bridge grows in the inertial regime at constant speed, and

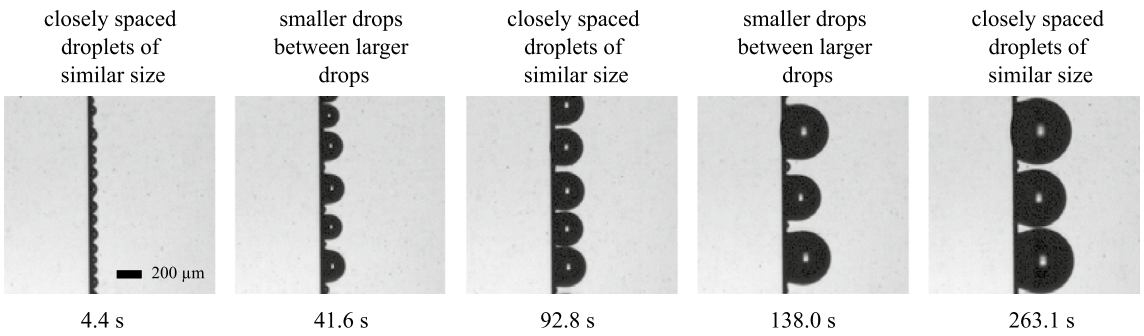

Fig. 11 Characteristic rows of drops on a fiber for the process of droplet growth

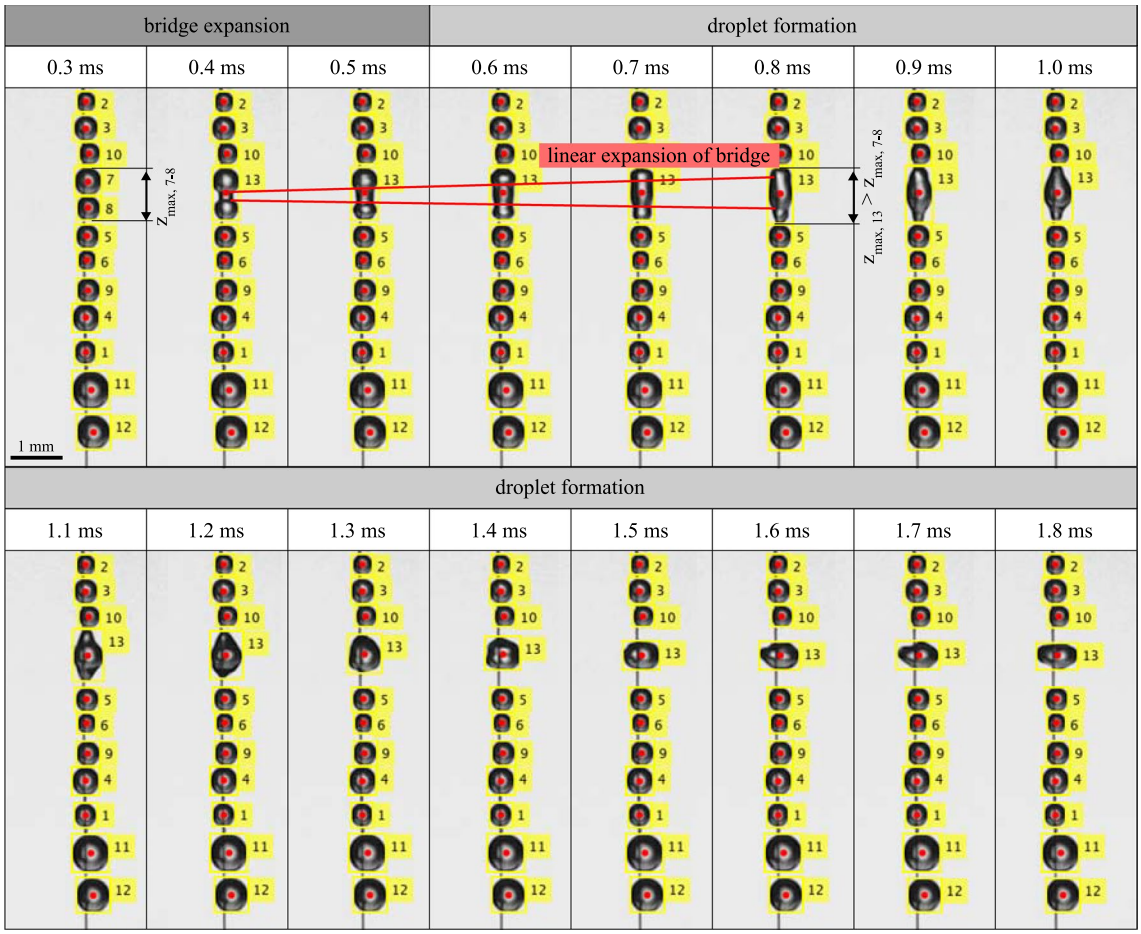

Fig. 12 Initial droplet coalescence caused by closely spaced growing droplets due to a continuous separation of water mist

the bridge expansion can be described by the propagation of non-dispersive capillary wave packets (Chireux et al. 2021).

In Fig. 12, the development of a cylindrical bridge between the droplets is clearly visible at t = 0.4 ms. The bridge has a radius of $R_B = 0.2$ mm at t = 0.4 ms and a $Oh_B << 1$ is received. The cylindrical shape of the bridge is maintained until t = 0.5 ms. Then, curvature of the bridge becomes reversed. The expansion rate of the bridge is approximately linear as marked in Fig. 12. Based on these findings, the here seen bridge development can be assigned to the inertial regime.

Chen et al. (2015) discovered that the linear inertial expansion of the liquid bridge transitions into a new linear but slower growth regime. In this regime, the orientation of the radiuses curvature of the bridge is reversed. We mark the point of change in curvature as the end of the bridge developing process and all further changes in shape of the droplet are referred to droplet deformation (see Fig. 12). Due to insufficient time resolution, we cannot distinguish between the two different growth regimes of the liquid bridge.

Many investigations have reported a droplet deformation in circumferential and longitudinal direction (Abouelsoud and Bai 2021; Deka et al. 2019; Chen et al. 2015; Li and Fritsching 2011; Mansouri et al. 2014). It is known that dynamic deformation occurs in the case of colliding and coalescing droplets. Deka et al. (2019) observed for unequal sized water droplets in air with neglectable collision speed that the longitudinal expansion of the droplet is wider than that of the two initial droplets.

Similar behavior can be seen in Fig. 12. At t = 0.8 ms, the vertical expansion of the droplet is wider than that of the two initial droplets 7 and 8 at t = 0.3 ms. This means that $z_{zmax,\ 13} > z_{zmax,\ 7\text{–}8}$ (see Fig. 12). This expansion is based on the movement of the capillary waves which focus energy at the tip of the droplet and therefore stretch the droplet (Deka et al. 2019; Blanchette and Bigioni 2006; Ray et al. 2010). The not mentioned numbered droplets seem not to change in size. This is due to the high framerate of 10.000 fps and relative to that a slow droplet growth by coalescence with the liquid aerosols contained in mist.

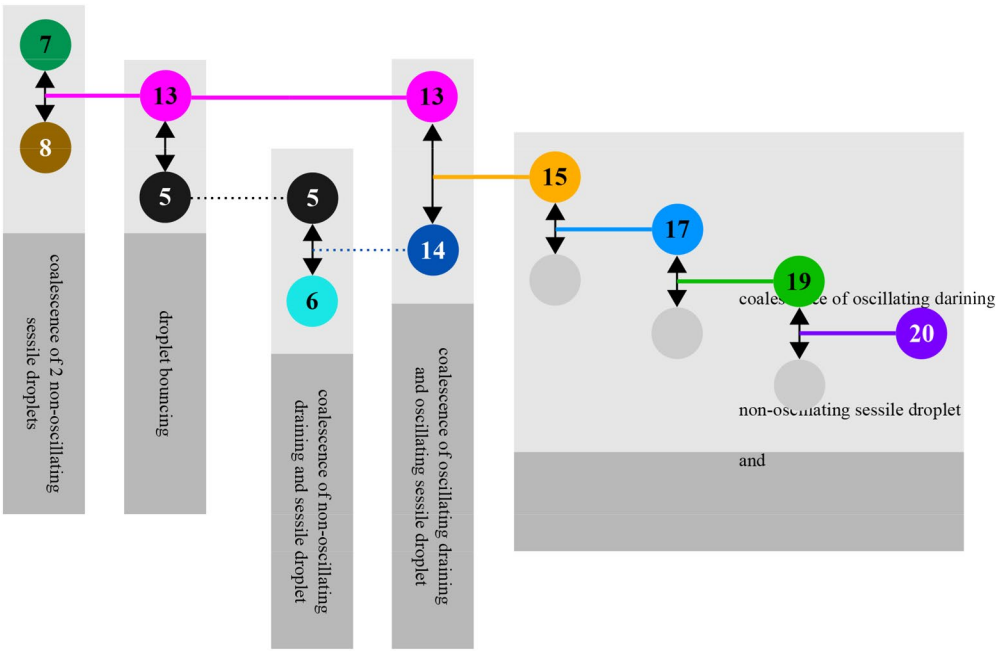

Fig. 13 Order of coalescence events

Further coalescence events follow when the draining droplet interacts with other droplets on its way down along the fiber.

The following shows the drainage process of a draining droplet along a fiber with a droplet chain. This is the drainage of the droplet 13 from Fig. 12 along the fiber shown there.

In Fig. 13, the coalescence events are put into the temporal order and assigned to a coalescence mechanism. The participating droplet of one coalescence event is numbered and represented by colored circles. TrackIDs that belong to one droplet are marked with a line in the same color. A new color was introduced whenever a new droplet was detected that could not be assigned to an existing TrackID, i.e., after coalescence events. Solid thick lines highlight the course of the major draining droplet.

The z-positions are plotted in Fig. 14 in order to get a better understanding of the time dependency. Solid thick lines show the z-position of the center of mass and the narrow vertical lines show the axial size z_{max} of all droplets for each frame during the entire recording time. Prominent TrackIDs in color highlight the course of the draining droplet.

The first expansion and contraction of droplet 13 in z-direction was shown by a series of images in Fig. 12. Further expansions and contractions are visible in Fig. 14 until droplet 13 coalesces again. A damping of the amplitude of z_{max} is clearly recognizable for TrackID 13.

More insights into the amplitude of z_{max} and x_{max} can be derived from Fig. 15. One can see logically a sudden increase in the z-amplitude at the beginning of each coalescence process. A decrease in amplitude can also be seen in subsequent amplitudes. We attribute this decrease in amplitude to the damping properties of water and the frictional losses of the droplet on the fiber. As the mass of the draining droplet increases through a coalescence event, the amplitude increases and the frequency of decreases. This increase in amplitude is best seen by comparing TrackID 13 and TrackID 15 in Fig. 15.

More detailed frequency investigations using Fourier transformation (FT) for TrackID 13, 15 and 19 show the decrease of the frequency with increasing mass of the draining droplet in Fig. 16. FT was only performed for these three tracks, as in this case an oscillation is present over at least one period. After initial coalescence, the dominant calculated frequency is 495 Hz for both the x- and y-directions of TrackID 13. After mass increase by further coalescence, the frequency for the x- and y-direction for TrackID 15 decreases to 385 Hz and for TrackID 19 to 333 Hz.

Neglecting the interaction of a spherical droplet with the fiber and assuming a frictionless and incompressible liquid for an isolated droplet, the natural frequency ω of this droplet for different modes n can be approximately determined with

$$\omega_n^2 = n(n-1)(n+2)\frac{\sigma}{\rho a_0^3} \tag{5}$$

as shown by Rensink (Huang and Pan 2021). The radius of a sphere of equal volume is denoted by a_0. The first natural frequency of a droplet whose surface deforms is $n = 2$. Here, the droplet surface performs vibrational movements, which it alternately converts into an oblate and a prolate spheroid form. In a good approximation, this oscillation behavior can be seen in Fig. 12 for droplet 13. This can also be assumed approximately for the oscillation of droplets 15 and 19, which are not depicted here. A comparison in Fig. 17 shows that the determined frequencies of droplet 13, 15 and 19 are below the analytically determined frequencies for an idealized droplet with $n = 2$. Additional results from replicate experiments confirm the lower measured frequency for droplet vibration on droplets attached to fibers compared to idealized droplets.

We attribute this deviation to the contact of the droplet with the fiber. This increases the surface area and disrupts vibration. A decrease in frequency with increasing volume after a coalescence event is consistent with Eq. (5). Detailed investigations into the oscillation frequency of droplets require the targeted application of defined droplet volumes to a fiber and are beyond the scope of this work.

A closer look into the onset of drainage shows that adhesive forces between droplet and fiber are reduced when the droplet oscillates. Droplet 11, with a diameter of $D = 0.84$ mm, is sessile during the entire observation time. If one assumes that the sessile droplet is perfectly round (which is not entirely correct but for this purpose a good assumption), then it would have a volume of 0.31 mm^3. Droplet 7 and 8 have with the same assumption a combined volume of 0.2 mm^3. These two droplets coalesce and form the oscillating draining droplet 13 like already described. Thus, the adhesive forces are reduced for an oscillating droplet compared to a sessile droplet and drainage can start at lower droplet masses as illustrated in Fig. 18. This seems plausible due to a reduced contact area in periods of reduced z_{max} during oscillation.

In the following, further coalescence mechanisms are described based on the observed coalescence events in the recorded timeframe.

We consider the here seen motion of droplet 5 in Fig. 19 to be based on droplet bouncing with droplet 13 analogue to the illustration in Fig. 1. It can be seen that the draining droplet 13 collides with the neighboring droplet 5 and sets it in motion instead of coalescing with it. The transport velocity of the center of mass of the oscillating draining droplet 13 is about 0.05 ms^{-1} right before contact with the adjacent droplet 5 and has a D_1 of 0.74 mm. The propagation speed of the droplet surface of the oscillating draining droplet 13 relative to the sessile droplet 5 averaged over same period of time from 8.7 ms to 9.1 ms is 0.12 ms^{-1}. With an averaged diameter of the smaller droplet 5 of $D_s = 0.52$ mm, a Weber

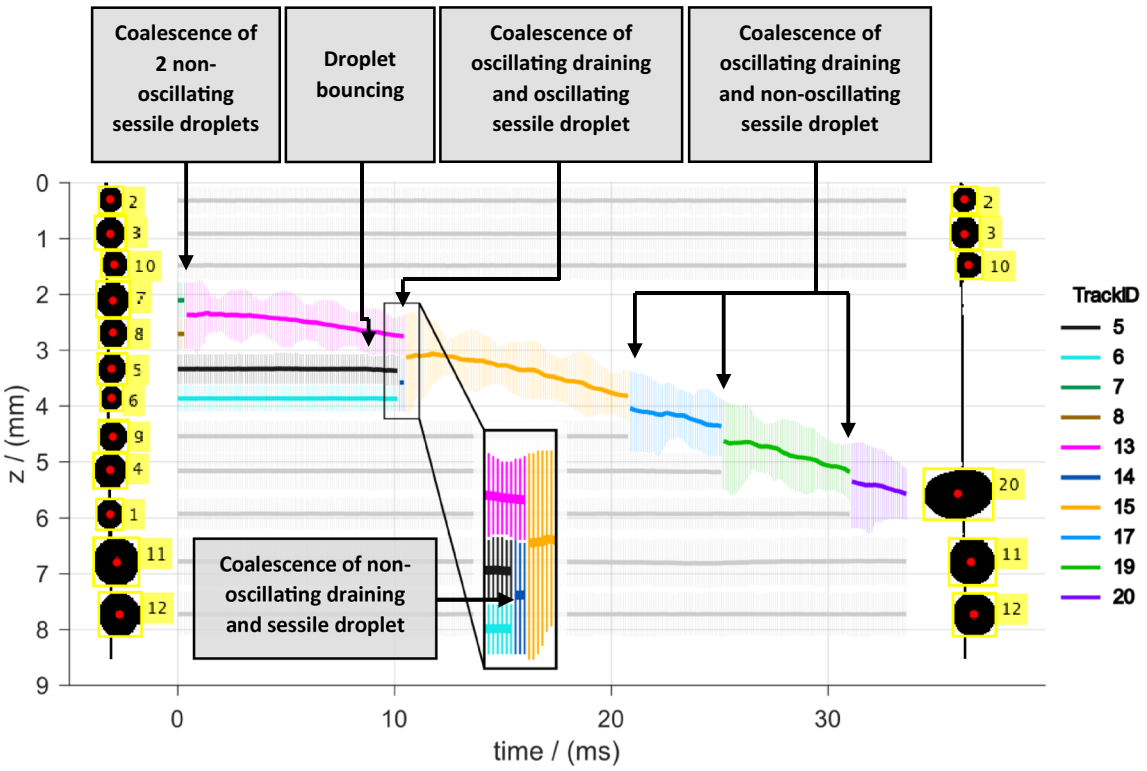

Fig. 14 Z-position and size of all detected droplets

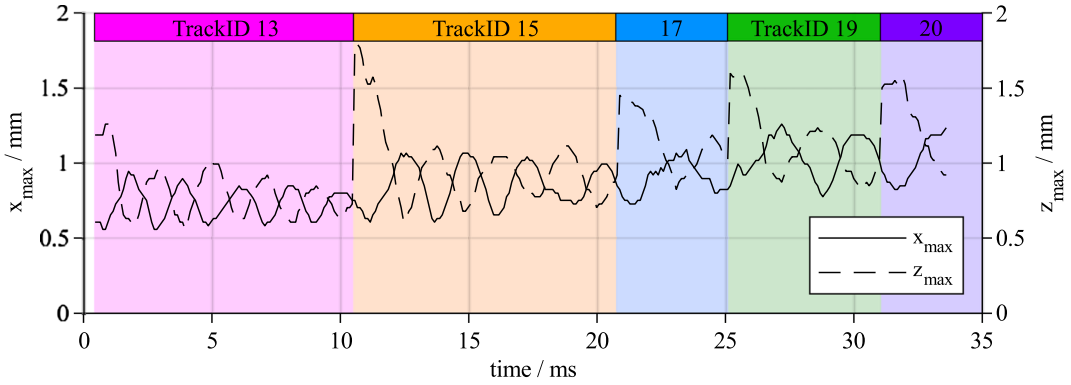

Fig. 15 Amplitude of x_{max} and z_{max} of the draining droplet

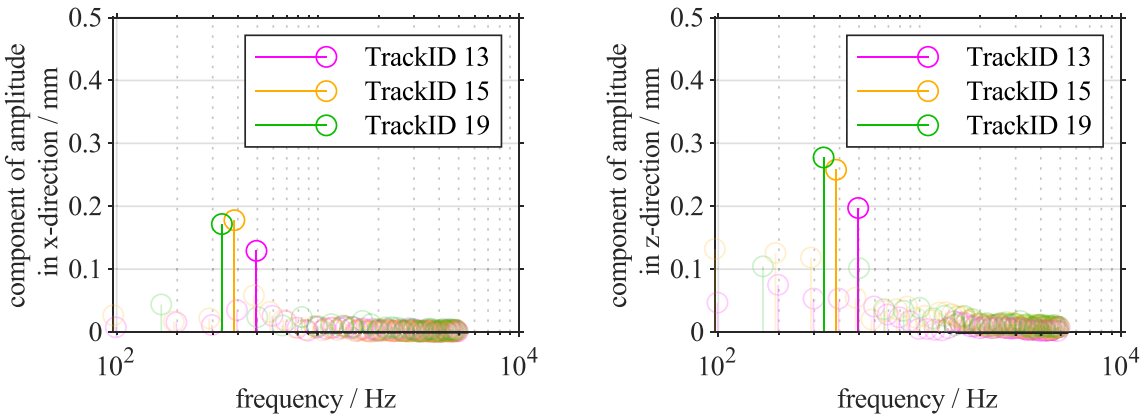

Fig. 16 The component of the amplitude for the frequency spectrum shown separately for the *x*- and *y*-direction

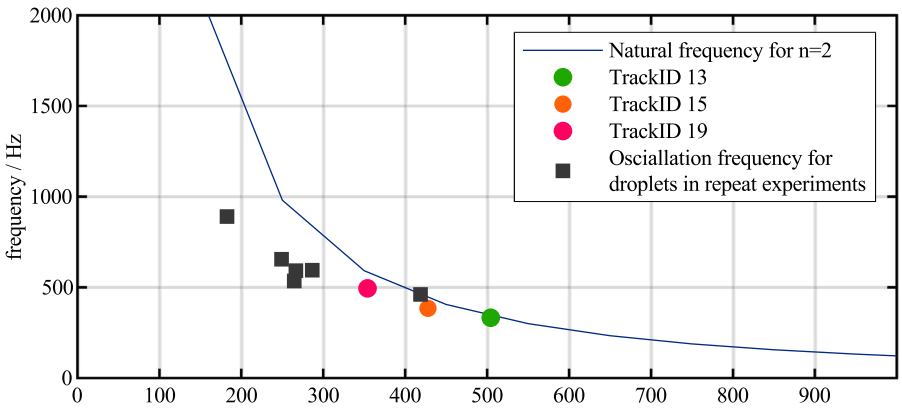

Fig. 17 Comparison of natural frequency with mode $n = 2$ and observed frequencies for oscillating droplets

number of We = 0.12 and a droplet ratio of $D_s/D_l = 0.7$ are determined. The averaged velocity of the center of mass of droplet 5, which is set into motion due to the bounce, is in the timeframe between 9.1 ms and 9.7 ms about 0.026 ms^{-1}. The movement is about 180 µm downward along the vertical fiber. The reduced velocity of droplet 5 of 0.026 ms^{-1} compared to droplet 13 of 0.05 ms^{-1} seems plausible due to the fact kinetic energy must be reduced in an elastic bounce.

The influence of the fiber on droplet bouncing remains uncertain but is expected to be neglectable when the droplet contact area is outside the fiber like for the bridging process mentioned already by Zhang et al. (Zhang et al. 2022). In Fig. 19, it is clearly visible that the fiber is off center of the contact area, but no statement can be made as to whether the fiber is also outside the contact area.

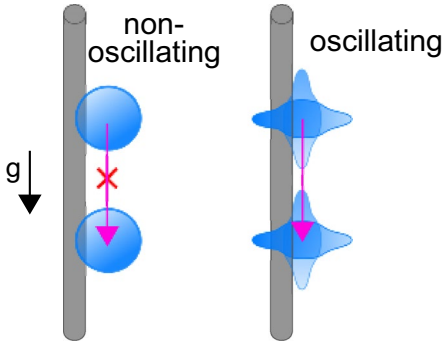

Fig. 18 Reduced adhesive forces due to oscillation

Repeat experiments show that 79.6% of the droplet collisions resulted in coalescence and 20.4% in droplet bouncing.

A selection of the observed droplet-droplet collisions is divided into coalescence and droplet bouncing in Fig. 20. The Weber number We and the impact parameter $B = \frac{D_l - D_s}{D_l + D_s}$ are assigned to each of these droplet collisions. B can be interpreted as the ratio of the distance between the normal of the velocity direction and the averaged diameter of the colliding droplets. The mass centers of droplets move toward each other on parallels (assuming that the droplets do not rotate around the fiber). If the two differently sized droplets are in the same position in the circumferential direction, the distance between the normal of the velocity direction is given with $\frac{D_l - D_s}{2}$. Since the position in the circumferential direction cannot be clearly determined from the perspective used, the actual distance of the parallel droplets remains unknown.

Furthermore, it should be noted that the average diameter was used for evaluation. For oscillating droplets, however, the surface curvature at the contact point can differ significantly from the surface curvature of a volume-equal sphere. Local radii can better describe the local curvature from a projection surface, but still neglect a second view to describe the curvature. In addition, local radii do not contain any information about the droplet volume, which is why an average diameter was used here.

The remarks on the curvature and the limitations from one viewing angle in combination with an undefined droplet placement make clear that droplet bouncing on a fiber should be examined under more defined boundary conditions with drops of defined position and size on a fiber. Nevertheless, important insights can be gained from the results shown here.

Huang and Pan (2021) were able to show droplets bouncing of isolated droplets for the first time under atmospheric pressure in a head-on collision for equally sized water droplets. With increasing droplet size, droplet bouncing was detected for smaller values of B. For We < 1, for both droplet diameters of 700 and 1000 µm, only coalescence and no droplet bouncing can be seen in their work.

In our results shown in Fig. 20, droplet bouncing is evident for We < 1. The differentiation between droplet bouncing and coalescence for smaller values of We (here We = [0.1; 0.8]) is given by a discontinuous function. The lowest We number at which droplet bouncing occurs is $B = 0.2$. In comparison, Huang and Pan (2021) show a continuous function as the boundary between droplet bouncing and coalescence. For them, the boundary shifts toward larger values of B as the Weber number decreases.

The differentiation between droplet bouncing and coalescence for larger values of We (here We = [2; 3]) can only be estimated by two collision events.

Figure 2 depicts the process of two oscillating droplets coalescing. Due to the movement of droplet 5 by droplet bouncing, droplets 5 and 6 coalesce into a new droplet 14 as shown in Fig. 21. Droplet 14 is observed in only 3 frames from 10.3 ms to 10.5 ms. Droplet 13 is the oscillating draining droplet and is transported in the z-direction right before

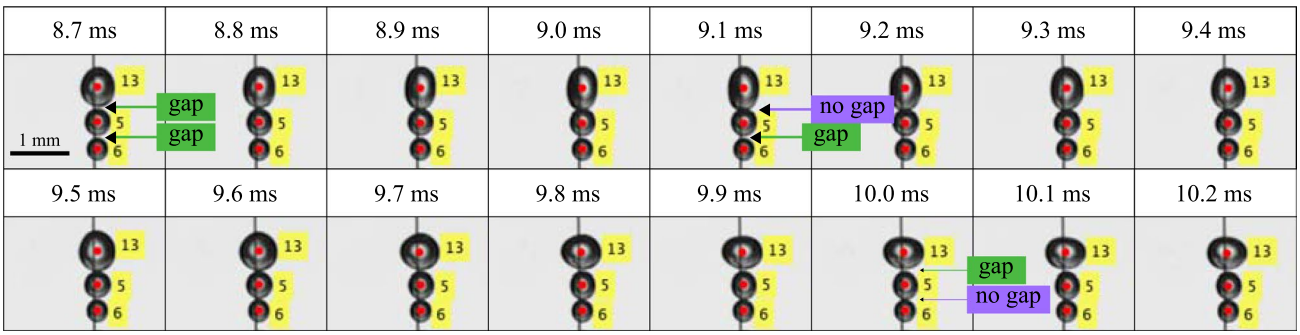

Fig. 19 Droplet bouncing: Droplet 13 pushes droplet 5 down the fiber

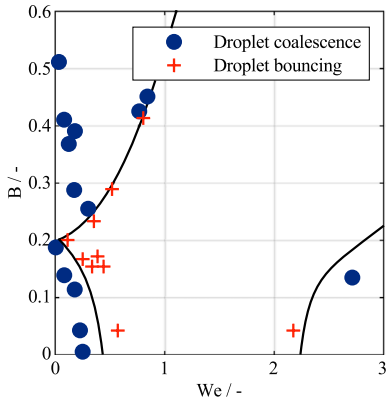

Fig. 20 Droplet coalescence (blue dot) and droplet bouncing (orange plus)

coalescing with droplet 14. Additionally, droplet 14 also deforms due to coalescence. If one considers coalescence events of two oscillating droplets, different characteristic states are possible. These characteristic states could be combinations in that the involved droplets have maximum/minimum expansion or maximum velocity of expansion/contraction. These states should be reproduced and investigated in future studies. The propagation speed of the droplet surface of the draining droplet based on the oscillation is relatively slow compared to the development of the bridge and inclusion of the smaller sessile drop. Therefore, the influence of the oscillation on the bridge development is assumed to play only a minor part.

As already shown, the draining droplet is subjected to an oscillating movement. While draining along the fiber, the oscillating droplet collects sessile droplets as illustrated in Fig. 2. This coalescence mechanism is shown exemplary in Fig. 22 for one coalescence event. Depending on the distance and state of deformation the collision can take place at distinct states of the deformed droplet, e.g., at maximum expansion in longitudinal or circumferential direction. The collision in Fig. 22 takes place during positive expansion rate in z-direction of the draining droplet. The oscillating draining droplet 19 has an averaged diameter of $D_d = 1.02$ mm. The non-oscillating sessile droplet 1 has an averaged diameter of $D_s = 0.52$ mm. Based on the diameter ratio of $D_1/D_s = 1.96$, a determined Oh_s of 0.0052 and the findings of Zhang et al. (2009), a satellite droplet is to be expected in Fig. 22. However, a formation of a satellite droplet could not be observed here (see Fig. 22). This is most likely due to the existence of the fiber which prevents the pinching at the bottleneck.

The transport of the liquid volume fraction of the smaller droplet along the fiber toward the larger droplet as illustrated in Fig. 1 is clearly visible during the described coalescence event seen in Fig. 22. Comparable behavior was shown by Chu et al. (2016). They investigated the droplet sweeping of several droplets of different sizes on a superhydrophobic surface and showed an increasing attracting effect of the larger droplet on the smaller droplet with increasing size difference, although no highly temporally resolved information was given.

5 Conclusions

In this paper, key mechanisms of droplet coalescence and droplet transport for the onset and during drainage along a vertical fiber were identified:

A) A draining droplet is subjected to oscillation in horizontal and vertical directions when coalescing with other droplets on a fiber.
B) Due to the oscillation of the droplet, adhesive forces between the fiber and droplet are reduced compared to a stationary droplet of identical size. Drainage can therefore start already at smaller droplet masses.
C) When two water droplets coalesce on a vertical fiber surrounded by air at atmospheric pressure, initial dimensions of the two droplets are smaller than those of the coalesced transient deforming droplet.
D) Droplet bouncing was observed for We = [0.0001; 1] at the given absolute pressure of 986.44±0.05 hPa.
E) The influence of the fiber is assumed to be neglectable at droplet bounce when the contact area of the droplets is beside the fiber.
F) Droplet sweeping was observed for unequal sized water droplets similar to the known behavior of droplet sweeping on flat surfaces.
G) The formation of a satellite droplet was not observed although it should exist for droplet sweeping based on

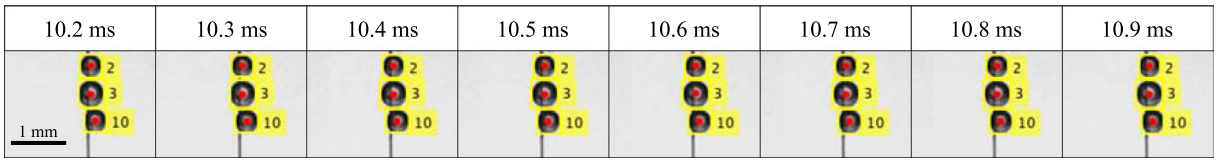

Fig. 21 Droplet 5 and 6 coalesce and form droplet 13. Droplet 13 therefore elongates and coalesce with the oscillating draining droplet

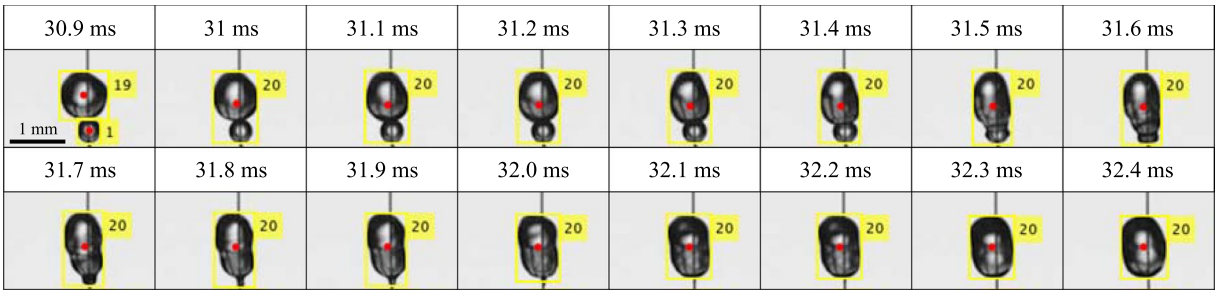

Fig. 22 Attracting effect of an oscillating draining droplet. The smaller collected droplet moves upward

the findings in the literature. The influence of the fiber might prevent the pinching. Further investigations are needed.

In future studies, the individual mechanisms are to be reproduced on the basis of single droplets on the fiber and the dependencies of key influencing parameters such as the oscillation frequency, amplitude and fiber parameters like diameter and wettability are to be determined.

Acknowledgements We wish to confirm that there are no known conflicts of interest associated with this publication. We confirm that the manuscript has been read and approved by all named authors and that there are no other persons who satisfied the criteria for authorship but are not listed. We further confirm that the order of authors listed in the manuscript has been approved by all of us. The authors have no relevant financial or non-financial interests to disclose. We gratefully acknowledge that this project was funded by the Deutsche Forschungsgemeinschaft (DFG, German Research Foundation) – DFG/499469405.

Author contributions A.S. conducted the experiments and analyzed the data. A.D. and J.M. contributed to the analysis of the data. A.S. wrote the paper with the input of all authors.

Funding Open Access funding enabled and organized by Projekt DEAL. This project was funded by the Deutsche Forschungsgemeinschaft (DFG, German Research Foundation)—DFG/499469405.

Data availability The datasets generated during and/or analyzed during the current study are available from the corresponding author on reasonable request.

Declarations

Conflict of interest The authors declare no conflict of interest.

References

Abouelsoud M, Bai B (2021) Bouncing and coalescence dynamics during the impact of a falling drop with a sessile drop on different solid surfaces. Phys Fluids 33(6):63309. https://doi.org/10.1063/5.0050829

Blanchette F, Bigioni TP (2006) Partial coalescence of drops at liquid interfaces. Nature Phys 2(4):254–257. https://doi.org/10.1038/nphys268

Chen Y, Shen C, Peterson GP (2015) Hydrodynamics and morphologies of droplet coalescence. Ind Eng Chem Res 54(37):9257–9262. https://doi.org/10.1021/acs.iecr.5b01459

Chireux V, Fabre D, Risso F, Tordjeman P (2015) Oscillations of a liquid bridge resulting from the coalescence of two droplets. Phys Fluids 27(6):62103. https://doi.org/10.1063/1.4922474

Chireux V, Tordjeman P, Risso F (2021) Bridge expansion after coalescence of two droplets in air: inertial regime. Phys Fluids 33(6):62112. https://doi.org/10.1063/5.0055238

Chu F, Wu X, Zhu B, Zhang X (2016) Self-propelled droplet behavior during condensation on superhydrophobic surfaces. Appl Phys Lett 108(19):194103. https://doi.org/10.1063/1.4949010

Dawar S, Chase GG (2008) Drag correlation for axial motion of drops on fibers. Sep Purif Technol 60(1):6–13

Dawar S, Chase GG (2010) Correlations for transverse motion of liquid drops on fibers. Sep Purif Technol 72(3):282–287. https://doi.org/10.1016/j.seppur.2010.02.018

Deka H, Biswas G, Chakraborty S, Dalal A (2019) Coalescence dynamics of unequal sized drops. Phys Fluids 31(1):12105. https://doi.org/10.1063/1.5064516

Finotello G, Padding JT, Deen NG, Jongsma A, Innings F, Kuipers JAM (2017) Effect of viscosity on droplet-droplet collisional interaction. Phys Fluids 29(6):67102. https://doi.org/10.1063/1.4984081

Gilet T, Terwagne D, Vandewalle N (2010) Droplets sliding on fibres. Eur Phys J E 31(3):253–262

Huang K-L, Pan K-L (2021) Transitions of bouncing and coalescence in binary droplet collisions. J Fluid Mech 928:A7. https://doi.org/10.1017/jfm.2021.797

Hurwitz M (2012) Modeling industrial coalescers: droplet dynamics: Droplet stability and coalescence problem. 28th annual workshop on, 2012. [Online]. Available: https://www.mathsci.

udel.edu/content-sub-site/Documents/MPI%202012/PallReport2012.pdf
Jin J, Ooi CH, Dao DV, Nguyen N-T (2017) Coalescence processes of droplets and liquid marbles. Micromachines 8(11):336. https://doi.org/10.3390/mi8110336
Kampa D, Wurster S, Buzengeiger J, Meyer J, Kasper G (2014) Pressure drop and liquid transport through coalescence filter media used for oil mist filtration. Int J Multiph Flow 58:313–324. https://doi.org/10.1016/j.ijmultiphaseflow.2013.10.007
Labbé R, Duprat C (2019) Capturing aerosol droplets with fibers. Soft Matter 15(35):6946–6951. https://doi.org/10.1039/c9sm01205b
Li XG, Fritsching U (2011) Numerical investigation of binary droplet collisions in all relevant collision regimes. J Comput Multiph Flows 3(4):207–224. https://doi.org/10.1260/1757-482X.3.4.207
Lycett-Brown D, Luo KH, Liu R, Lv P (2014) Binary droplet collision simulations by a multiphase cascaded lattice Boltzmann method. Phys Fluids 26(2):23303. https://doi.org/10.1063/1.4866146
Mansouri A, Arabnejad H, Mohan RS (2014) Numerical investigation of droplet-droplet coalescence and droplet-interface coalescence In: Fluids engineering division summer meeting collocated with the asme 2014 12th international conference on nanochannels, microchannels, and minichannels https://doi.org/10.1115/FEDSM2014-21642
Mead-Hunter R, Bergen T, Becker T, O'Leary RA, Kasper G, Mullins BJ (2012) Sliding/rolling phobic droplets along a fiber: measurement of interfacial forces. Langmuir 28(7):3483–3488. https://doi.org/10.1021/la2046838
Mead-Hunter R, King AJ, Kasper G, Mullins BJ (2013) Computational fluid dynamics (CFD) simulation of liquid aerosol coalescing filters. J Aerosol Sci 61:36–49. https://doi.org/10.1016/j.jaerosci.2013.03.009
Mullins BJ, Braddock RD, Agranovski IE, Cropp RA, O'Leary RA (2005) Observation and modelling of clamshell droplets on vertical fibres subjected to gravitational and drag forces. J Colloid Interface Sci 284(1):245–254. https://doi.org/10.1016/j.jcis.2004.10.013
Mullins BJ, Pfrang A, Braddock RD, Schimmel T, Kasper G (2007) Detachment of liquid droplets from fibres—experimental and theoretical evaluation of detachment force due to interfacial tension effects. J Colloid Interface Sci 312(2):333–340
Ojaghlou N, Tafreshi HV, Bratko D, Luzar A (2018) Dynamical insights into the mechanism of a droplet detachment from a fiber. Soft Matter 14(44):8924–8934. https://doi.org/10.1039/C8SM01257A
Pan Y, Suga K (2005) Numerical simulation of binary liquid droplet collision. Phys Fluids 17(8):82105. https://doi.org/10.1063/1.2009527
Pan K-L, Law CK, Zhou B (2008) Experimental and mechanistic description of merging and bouncing in head-on binary droplet collision. J Appl Phys 103(6):64901. https://doi.org/10.1063/1.2841055
Paulsen JD (2013) Approach and coalescence of liquid drops in air. Phys Rev E Stat Nonlinear Soft Matter Phys 88(6):63010. https://doi.org/10.1103/PhysRevE.88.063010
Paulsen JD, Burton JC, Nagel SR (2011) Viscous to inertial crossover in liquid drop coalescence. Phys Rev Lett 106(11):114501. https://doi.org/10.1103/PhysRevLett.106.114501
Paulsen JD, Burton JC, Nagel SR, Appathurai S, Harris MT, Basaran OA (2012) The inexorable resistance of inertia determines the initial regime of drop coalescence. Proc Natl Acad Sci USA 109(18):6857–6861. https://doi.org/10.1073/pnas.1120775109
Qian J, Law CK (1997) Regimes of coalescence and separation in droplet collision. J Fluid Mech 331:59–80. https://doi.org/10.1017/S0022112096003722
Ray B, Biswas G, Sharma A (2010) Generation of secondary droplets in coalescence of a drop at a liquid–liquid interface. J Fluid Mech 655:72–104. https://doi.org/10.1017/S0022112010000662
Straube C, Meyer J, Dittler A (2021) Identification of deposited oil structures on thin porous oil mist filter media applying µ-ct imaging technique. Separations 8(10):193. https://doi.org/10.3390/separations8100193
Tang C, Zhang P, Law CK (2012) Bouncing, coalescence, and separation in head-on collision of unequal-size droplets. Phys Fluids 24(2):22101. https://doi.org/10.1063/1.3679165
Thoroddsen ST, Takehara K, Etoh TG (2005) The coalescence speed of a pendent and a sessile drop. J Fluid Mech 527:85–114. https://doi.org/10.1017/S0022112004003076
Zhang FH, Li EQ, Thoroddsen ST (2009) Satellite formation during coalescence of unequal size drops. Phys Rev Lett 102(10):104502. https://doi.org/10.1103/PhysRevLett.102.104502
Zhang K, Liu F, Williams AJ, Qu X, Feng JJ, Chen CH (2015) Self-propelled droplet removal from hydrophobic fiber-based coalescers. Phys Rev Lett 115(7):074502. https://doi.org/10.1103/PhysRevLett.115.074502
Zhang Y, Yan S, Yang X, Bai Z (2022) Hydrodynamics and morphologies of droplets coalescence on fiber. AIChE J. https://doi.org/10.1002/aic.17673